Neoplasma 2023; 70(3): 402–415

doi:10.4149/neo_2023_230319N155

TRIM31 promotes the progression of oral squamous cell carcinoma through upregulating AKT phosphorylation and subsequent cellular glycolysis

Sheng-Qi SANG[1,#], Yi-Jie ZHAO[1,#], Meng WANG[1,2], Xiao-Qi ZHONG[1,2], Zhi-Cheng YANG[1,2,*], Meng-Meng LU[1,2,*]

[1]Shanghai Key Laboratory of Craniomaxillofacial Development and Diseases, Fudan University, Shanghai, China; [2]Department of Oral and Maxillofacial Surgery, Shanghai Stomatological Hospital and School of Stomatology, Fudan University, Shanghai, China

**Correspondence: lumengmeng_kq@fudan.edu.cn; zhicheng_yang1998@fudan.edu.cn*
#Contributed equally to this work.

Received March 19, 2023 / Accepted June 26, 2023

The regulation of protein kinase B (AKT) phosphorylation by Tripartite motif-containing protein 31 (TRIM31) is implicated as an essential mechanism in the progression of many malignant tumors. Nevertheless, the function of the TRIM31/AKT pathway in oral squamous cell carcinoma (OSCC) remains elusive. Here, immunohistochemistry analysis of human OSCC tissue microarrays indicated significantly higher levels of TRIM31 and phosphorylated AKT (p-AKT) in OSCC tumors than in adjacent tissue samples. Also, we detected a positive association between TRIM31 expression and clinical OSCC development. In *in vitro* studies, TRIM31 knockdown severely impaired OSCC cell growth, invasion, and migration. By contrast, TRIM31 overexpression improved these cell behaviors, while subsequent AKT inhibition abrogated the effect. *In vivo* tumorigenesis experiments using nude mice also validated the effects of TRIM31/AKT signaling in tumor growth. Furthermore, TRIM31 upregulation facilitated glucose uptake, as well as lactate and adenosine triphosphate production of OSCC cells, while such positive effects on glycolysis and malignant cell phenotypes were reversed by treatment with AKT or glycolysis inhibitors. In conclusion, TRIM31 may improve OSCC progression by enhancing AKT phosphorylation and subsequent glycolysis. Hence, TRIM31 has the potential as a treatment target in OSCC.

Key words: TRIM31; AKT phosphorylation; oral squamous cell carcinoma; malignant cell behaviors; cellular glycolysis

Oral squamous cell carcinoma (OSCC) comprises approximately 3% of adult malignant tumors and is among the most common oral and maxillofacial malignancies [1]. The incidence of OSCC has been rising in recent years, with around half a million new patients worldwide annually [2]. Although surgical resection combined with radiotherapy and chemotherapy, targeted therapy, and immunotherapy have achieved some curative effects, the 5-year survival rate of patients with OSCC is < 60%, owing to tumor cell metastasis [3]. Given the lack of highly effective treatments, further understanding of OSCC tumorigenesis is highly significant, with the aim of discovering novel therapeutic targets and approaches.

Tripartite motif-containing protein 31 (TRIM31) is a TRIM protein family member, which features conserved RING-finger, coiled-coil, and B-box domains [4]. TRIM31 contributes to numerous biological processes, including gene transcription [5], protein ubiquitination [6], and regulation of cell behaviors [7]. Importantly, TRIM31 is a crucial regulator of the development of several cancers, including hepatocellular carcinoma [8], gallbladder cancer [9], and colorectal cancer [4]; however, the role of the TRIM31 molecular pathway in OSCC progression remains unclear.

Protein kinase B (AKT) signaling is pivotal in directing numerous cellular activities [10, 11], and phosphorylated AKT (p-AKT) has important roles in the growth, migration, and metabolism of cancer cells [6, 9, 12]. Also, p-AKT can promote cellular glycolysis, and stimulate adenosine triphosphate (ATP) and lactate production, to provide sufficient materials for biosynthesis [12], and the participation of p-AKT in glycolysis is considered to be among the most important biological mechanisms that facilitate cancer development [12, 13].

Increased p-AKT levels have been detected in OSCC, as well as a positive association between AKT phosphorylation and the degree of OSCC malignancy [14]. The TRIM31/AKT pathway has key roles in mediating tumor cell phenotypes in breast cancer and glioblastoma [5, 15]. Together, the above

findings indicate that exploration of TRIM31 and p-AKT functions and related molecular mechanism in OSCC progression is warranted.

In this study, TRIM31 and p-AKT expression patterns were evaluated in OSCC tissue microarrays, and their importance to the clinicopathological characteristics of individuals with OSCC was analyzed. Additionally, we used *in vitro* and *in vivo* assays to analyze the relationship between TRIM31, p-AKT, and glycolysis in OSCC development. Our results show that the TRIM31/AKT pathway may regulate cellular glucose metabolism and subsequent OSCC cell behaviors, thus influencing OSCC progression.

Patients and methods

Human OSCC tissue microarrays, OSCC cell lines, and culture. Commercial OSCC tissue microarrays (HN058OC01), including 39 primary OSCC tumor samples from tongue, buccal mucosa, and gingiva; 9 samples of OSCC-adjacent tissue; and 7 normal mucosa samples, were purchased from Zhongke Guanghua (Xi'an) Intelligent Biotechnology Co., Ltd. Tissue microarrays were provided with clinicopathological data from the cases, including sex, lymph node metastasis, and TNM stage.

Four human OSCC cell lines (Fadu, CLA27, HSC3, and HSC6) were acquired from the Cell Bank of Shanghai Institute of Cell Biology, Chinese Academy of Sciences. CAL27 and Fadu cell lines were cultivated in Dulbecco's modified Eagle's medium (DMEM; HyClone, Logan, UT, USA), while HSC3, HSC6, and human oral epithelial cell (HOEC) lines were cultivated in minimum essential medium (HyClone, Logan, UT, USA), supplemented with 10% fetal bovine serum (FBS) (Life Technology, Grand Island, NY, USA) and 1% combined streptomycin and penicillin antibiotics, in a humidified incubator with 5% CO_2 at 37 °C.

Immunohistochemical (IHC) staining and analysis of OSCC tissue microarrays. IHC staining was conducted to identify TRIM31 and p-AKT expression levels in OSCC tissue microarrays. Briefly, anti-TRIM31 (1: 500, Ab67785, Abcam, Cambridge, MA, USA) or anti-p-AKT (1: 1000, #9272, Cell Signaling Technology, Beverly, MA, USA) antibodies were incubated with the cancer microarrays overnight at 4 °C. After washing three times, microarrays were treated with secondary antibody for 30 min at 25 °C. IHC images were captured using a microscope (CX41RF, OLYMPUS, Tokyo, Japan). The following parameters were determined: 1) Positive area score (%), defined as the percentage of positively stained area in a section and counted using the ImageJ Fiji program (National Institutes of Health, Bethesda, MD, USA) [16]. 2) Positive cells score (%), defined as positively stained cell percentage in a sector, scored automatically using ImageJ Fiji software, and recorded as 0% = 0; 1–24% = 1; 25–50% = 2; 51–75% = 3; and 76–100% = 4 [17, 18]. 3) Staining intensity score, referring to staining intensity was scored by assessing average cell cytoplasm and nucleus staining intensity (ImageJ Fiji), where scores of three, two, one, and zero represent intense, moderate, mild, and no staining, respectively [17, 18]. 4) IHC scores, calculated by multiplying 'positive cells' and 'staining intensity' scores. IHC score <6 was considered to indicate low TRIM31/p-AKT expression, while IHC score ≥6 indicated increased expression [17, 18]. Moreover, specific clinical manifestations of cases were examined to identify associations between TRIM31 levels and OSCC development.

Quantitative real-time polymerase chain reaction (qRT-PCR). To determine the mRNA expression levels in human OSCC and HOEC cells, qRT-PCR was conducted. TRIzol reagent (1596-026, Invitrogen, Carlsbad, CA, USA) was employed to obtain total RNA, which was then dissolved in RNAse-free H_2O and preserved at –80 °C. cDNA was generated from RNA sample aliquots (1 μg) using a Fermentas Reverse Transcription kit (Fermentas, Hanover, MD, USA), and used as a template for qRT-PCR assays conducted with a SYBR Green PCR kit (#K0223, Thermo, Waltham, MA, USA) on an ABI-7300 real-time detector (ABI, Los Angeles, CA, USA). Reactions comprised pre-denaturation (10 min, 95 °C) followed by 40 rounds of denaturation, annealing, and elongation for 15 s at 95 °C, 45 s at 60 °C, and 60 s at 60 °C, respectively. Glyceraldehyde-3-phosphatedehydrogenase (*GAPDH*) served as the internal control for the calculation of relative gene expression levels using the ΔCT technique ($^{2-\Delta\Delta}$CT). The following primer sequences were used: *TRIM31* (F: 5'-AAGGAAGAACGCAATCAG-3' and R: 5'-TCGCAGAAATAGTGGAAC-3') and *GAPDH* (F: 5'-AATCCCATCACCATCTTC-3' and R: 5'-AGGCTGTTGTCATACTTC-3').

Western blotting assay. Radioimmunoprecipitation assay lysis buffer kit (BYL40825, JRDUN Biotechnology, Shanghai, China) was used to prepare lysates from cell lines for western blotting analysis. A bicinchoninic acid protein quantification kit (23225, Thermo, Waltham, MA, USA) was used to measure protein quantities. Equal quantities (20 μg) of protein samples extracted from cells were separated by sodium dodecyl sulfate-polyacrylamide gel electrophoresis and then transferred to polyvinylidene difluoride membranes. Membranes were treated with primary antibodies diluted in tris-buffered saline tween (TBST) buffer overnight at 4 °C. Antibodies against target proteins included: TRIM31 (1:500, Ab67785, Abcam, Cambridge, MA, USA), AKT (1:1000, #4060, Cell Signaling Technology, Danvers, MA, USA), p-AKT (1:800, #9272, Cell Signaling Technology, Danvers, MA, USA), hexokinase 2 (HK2) (1:1000, Ab209847, Abcam, Cambridge, MA, USA), glucose transporter 1 (GLUT1) (1:5000, Ab115730, Abcam, Cambridge, MA, USA), and GAPDH (1:5000, 60004-1-Ig, Proteintech, Wuhan, China). To remove unbound primary antibodies, membranes were washed three times in TBST buffer for 5 min each. Membranes were then incubated with horseradish peroxidase (HRP)-conjugated goat anti-rabbit secondary antibodies (IgG-HRP, 1:5000, ZB-2301, Zhong-

shan Golden Bridge Biotechnology, Beijing, China) for 1 h at room temperature, followed by three further washes with TBST buffer. Finally, High-sig enhanced chemiluminescence (Tanon 5200, Tanon Science and Technology Co., Ltd., Shanghai, China) was used to visualize blot signals. Semi-quantitative analysis was used to determine the level of expression of each protein; all protein blot densities were standardized to that of GAPDH.

Cell transfection and inhibitor treatment. pLKO.1-puro lentiviral vector (Addgene, Cambridge, MA, USA) was used to clone specific small hairpin RNA (ShRNA) sequences targeting *TRIM31* mRNA (Sangon Biotech Co., Ltd., Shanghai, China). The sequences of the Sh-TRIM31s were as follows: Sh-TRIM31-1 (456-465, 5'-GGAGAAGGAGACAGUACAAGU-3'), Sh-TRIM31-2 (519-528, 5'-GGUAGAACAUGAGAAGCAAAG-3'), Sh-TRIM31-3 (582-591, 5'-GGAGCGAGCUCUCAGGAUACG-3'). Specific coding sequences (CDS) of *TRIM31* were cloned in the pCDNA3.1(+) vector (Addgene, Cambridge, MA, USA), with the primers, F: (F: 5'-CGGCTAGCATGGCCAGTGGGCAGTTTGT-3' and R: 5'-CCCTCGAGCACTCCAAGGAAGTTCGATT-3'). To knock down the TRIM31 expression, human OSCC cells (3×10^5/well) were transfected with 1.5 μl of pLKO.1-puro-Sh-TRIM31, or blank pLKO.1-puro lentiviral vector as the negative control (Sh-NC), in 6-well plates and incubated for 6 h. Cells (3×10^5/well in 6-well plates) were transduced with either pCDNA3.1(+)-TRIM31 or a blank pCDNA3.1(+) vector as the negative control (Vector), and then incubated for 6 h. qRT-PCR and western blotting assays were employed to assess the transfection efficiency.

Sh-TRIM31-transfected cells (Sh-TRIM31) were treated with 10 μM AKT activator (SC-79) (S786303, Sellect, Houston, TX, USA) for 24 h. Cells overexpressing TRIM31 (Oe-TRIM31) were also incubated in the presence of AKT (LY294002) (Ab120243, Abcam, Cambridge, MA, USA) or glycolysis (2-DG) (GC17430, GlpBio, Montclair, CA, USA) inhibitors. OSCC cells that had undergone different treatments were used for *in vitro* cell behavior and glycolysis, and *in vivo* tumorigenesis assays.

Cell proliferation assay. Cell counting kit-8 (CCK-8) (C0038, Beyotime, Shanghai, China) was used to measure OSCC cell growth. Cells (5×10^3/well) were seeded in 96-well microplates, left to adhere overnight in a humidified 5% CO_2 incubator at 37 °C, and then regularly monitored. Cells were supplemented with CCK-8 at 0, 12, 24, and 48 h following transfection and then kept at 37 °C for 1 h. Absorbance values (optical density) at 450 nm were determined for each well using a microplate reader (DNM-9602, Perlong, Beijing, China).

Transwell invasion assay. OSCC cell invasion tests were conducted using Transwell chambers (3422, COSTAR, Cambridge, MA, USA). Target cells resuspended at 3×10^5 cells/ml in a medium without FBS were introduced to the upper chambers, then DMEM containing 10% FBS was added into the lower chambers. Following two days of culture, cells were immediately fixed at room temperature by adding 4% formaldehyde for 15 min. Fixed cells were washed in phosphate-buffered saline (PBS) before staining for 30 min with 0.1% crystal violet staining solution; a microscope (CX41RF, OLYMPUS, Tokyo, Japan) was used to view and count cells.

Wound healing assay. Wound healing tests were employed to evaluate OSCC cell migration. Cells (5×10^3/well) were seeded in 6-well plates and wound-healing experiments were conducted by scratching through the cell monolayer with a sterile pipette tip after the cells had achieved confluence. To remove non-adherent cells, plates were washed twice with PBS. Then, cells were grown in a fresh medium for 48 h. At 0, 24, and 48 h, images were taken using a microscope (CX41RF, OLYMPUS, Tokyo, Japan). Cell migration rates were calculated as:

Cell migration rate (%) = ((scratch area at 0 h – scratch area at 48 h)/ scratch area at 0 h) × 100%.

Nude mouse tumorigenesis assay, IHC, Hematoxylin and Eosin staining. The Institutional Animal Care and Use Committee of Shanghai Rat & Mouse Biotech Co., Ltd. (SHRM-IACUC-022) authorized all animal research, which was conducted based on the National Research Council's Guide for the Care and Use of Laboratory Animals. The Shanghai Model Organisms Center, Inc. provided 30 6-week-old female BALB/c nude mice. Mice were randomly assigned to five groups, as follows: 1) Vector, 2) Sh-TRIM31, 3) Sh-TRIM31+SC-79, 4) Oe-TRIM31, 5) Oe-TRIM31+LY294002. OSCC cells treated with empty vector, Sh-TRIM31, and TRIM31-CDS were introduced subcutaneously into the right flanks of mice in the Vector, Sh-TRIM31, and Oe-TRIM31 groups, respectively; AKT activator (SC-79) and AKT inhibitor (LY294002) were simultaneously injected into mice in the Sh-TRIM31+SC-79 and Oe-TRIM31+LY294002 groups, respectively. Every three days, the development of subcutaneous tumors was observed. Tumor volume was calculated as length × width^2/2. Thirty days following the injection, mice were euthanized and tumor tissues were collected and weighed.

To verify the TRIM31 expression, IHC staining was applied to tumor tissue specimens. Specimens were fixed for 48 h in 10% formaldehyde, then embedded in paraffin, and 5 μm sections were cut from the tissue blocks. Slides were heated for 30 min at 65 °C, then deparaffinized with xylene, and rehydrated with a series of ethanol solution concentrations. Antigen retrieval was conducted in 0.01 M citrate buffer at 95 °C and samples were blocked with 5% bovine serum albumin for 30 min. Samples were stained for TRIM31 protein using the protocol described in section 2.2 (Immunohistochemical (IHC) staining and analysis of OSCC tissue microarrays) above.

The residual tumor samples were preserved in ethanol and paraffin-embedded after being fixed in 10% formaldehyde for 48 h. Hematoxylin and eosin (#714094, BASO, Zhuhai, China) staining was used to stain tissue sections mounted

on slides for examination using a microscope (CX41RF, OLYMPUS).

Ethics statement. All animal experiments followed the National Research Council's Guide for the Care and Use of Laboratory Animals and were approved by the Institutional Animal Care and Use Committee of Shanghai Rat &Mouse Biotech CO., Ltd. (SHRM-IACUC-022).

Glucose uptake assay. To evaluate the glucose uptake rate of OSCC cells, a 2-deoxy-2-[(7-nitro-2,1,3-benzoxadiazol-4-yl) amino]-D-glucose (2-NBDG) Glucose Uptake Assay Kit (K682-50, Biovision, Milpitas, CA, USA) was used, following the manufacturer's instructions. In summary, cells (3×10^5/well) were seeded in 6-well plates and incubated for one day. After removing the culture medium, PBS containing 100 μmol/l of the fluorescent glucose analog, 2-NBDG, was added for 1 h. Free 2-NBDG was removed by washing twice with cold PBS. Cells were then stained with 5 mg/ml propidium iodide (PI) for 30 min at 37 °C, then lysed with 0.25% trypsin-ethylenediaminetetraacetic acid (Solarbio, Beijing, China), followed by flow cytometry to examine 2-NBDG-positive and PI-negative cells (FACSAria III, BD Biosciences, Durham, NC, USA).

ATP production assay. Cellular ATP levels were quantified using ATP detection kits (A095, Jiancheng, Nanjing, China). Six-well plates were seeded with cells (5×10^5/well). Following a 48 h incubation period, 20 μl aliquots of cell supernatant were obtained and combined with the identification reagent following the manufacturer's recommendations. Following incubation at 37 °C for 10 min, absorbance at 530 nm was determined using a microplate reader (DNM-9602, Perlong), and ATP levels were determined using the formula provided by the kit manufacturer.

Lactate colorimetric assay. Lactate assay kits (A019-2, Jiancheng, Nanjing, China) were used to measure lactate levels in OSCC cells. Cells (5×10^5/well) were seeded into 6-well plates. After incubation for 48 h, cell supernatant aliquots (20 μl) were mixed with detection reagent, following the manufacturer's protocol, and after incubation at 37 °C for 10 min, absorbance measured at 530 nm using a microplate reader (DNM-9602, Perlong). Lactate concentrations were determined using the formula provided by the kit manufacturer.

Statistical analysis. All graphs were generated using GraphPad Prism (version 8.0, San Diego, CA, USA), and statistical analyses were conducted using SPSS (version 21, Chicago, IL, USA). Clinicopathological data from OSCC tissue microarrays were analyzed using the Chi-square test. Spearman correlation tests were conducted to analyze the relationships between OSCC clinical manifestations and TRIM31 expression levels. Data from *in vitro* assays using OSCC cells and *in vivo* experiments were examined by one-way analysis of variance (ANOVA) combined with Tukey's post-hoc test. All results from three independent trials are presented as mean ± standard deviation. A p-value <0.05 was considered statistically significant.

Table 1. Basic information and clinical manifestations of patients with high and low expressions of TRIM31 from OSCC tissue microarrays.

Clinical manifestation	TRIM31 expression in the OSCC tissues		p-value
	High (n)	Low (n)	
Sex			0.947
Male	29	8	
Female	1	1	
Age (yrs)			0.154
<60	23	4	
≥60	7	5	
Tumor size (cm)			0.044
<4	17	9	
≥4	13	0	
T classification			0.048
T1,2	10	7	
T3,4	20	2	
TNM stage (AJCC)			0.011
Stage I, II	10	8	
Stage III, IV	20	1	
Lymph node metastasis			0.021
Absent	15	9	
Present	15	0	

Abbreviation: AJCC-American Joint Committee on Cancer

Results

TRIM31 and p-AKT expression levels are upregulated in human OSCC tissues, and associated with clinical manifestations of patients with OSCC. To investigate the TRIM31 and p-AKT protein expression levels in human OSCC, we performed IHC staining of tissue microarrays, comprising OSCC tumor and adjacent tissue samples. Both TRIM31 and p-AKT were positively stained brown in the cell cytoplasm and nucleus. In comparison to cells of the adjacent tissues, tumor cells with high expression of TRIM31 and p-AKT appeared pleomorphic with obviously increased mitotic activity, while such characteristics of lowly-expressing cells slightly increased (Figure 1A). Positive area and cell percentages, as well as IHC scores for TRIM31 (Figures 1B, 1D) and p-AKT (Figures 1C, 1D) were clearly higher in human OSCC tumors than in corresponding adjacent tissue samples. Overall, p-AKT and TRIM31 expression levels in the tissue types were positively correlated with one another, and the results from tumor, adjacent, and normal tissues were partially overlapped (Figure 1E).

We also analyzed whether there were associations between the clinical manifestations of patients with OSCC and TRIM31 expression in the tissue microarrays. As illustrated in Table 1, TRIM31 expression levels were significantly increased in patients with larger tumor size, higher T and TNM stage, and more lymph node metastasis. Consis-

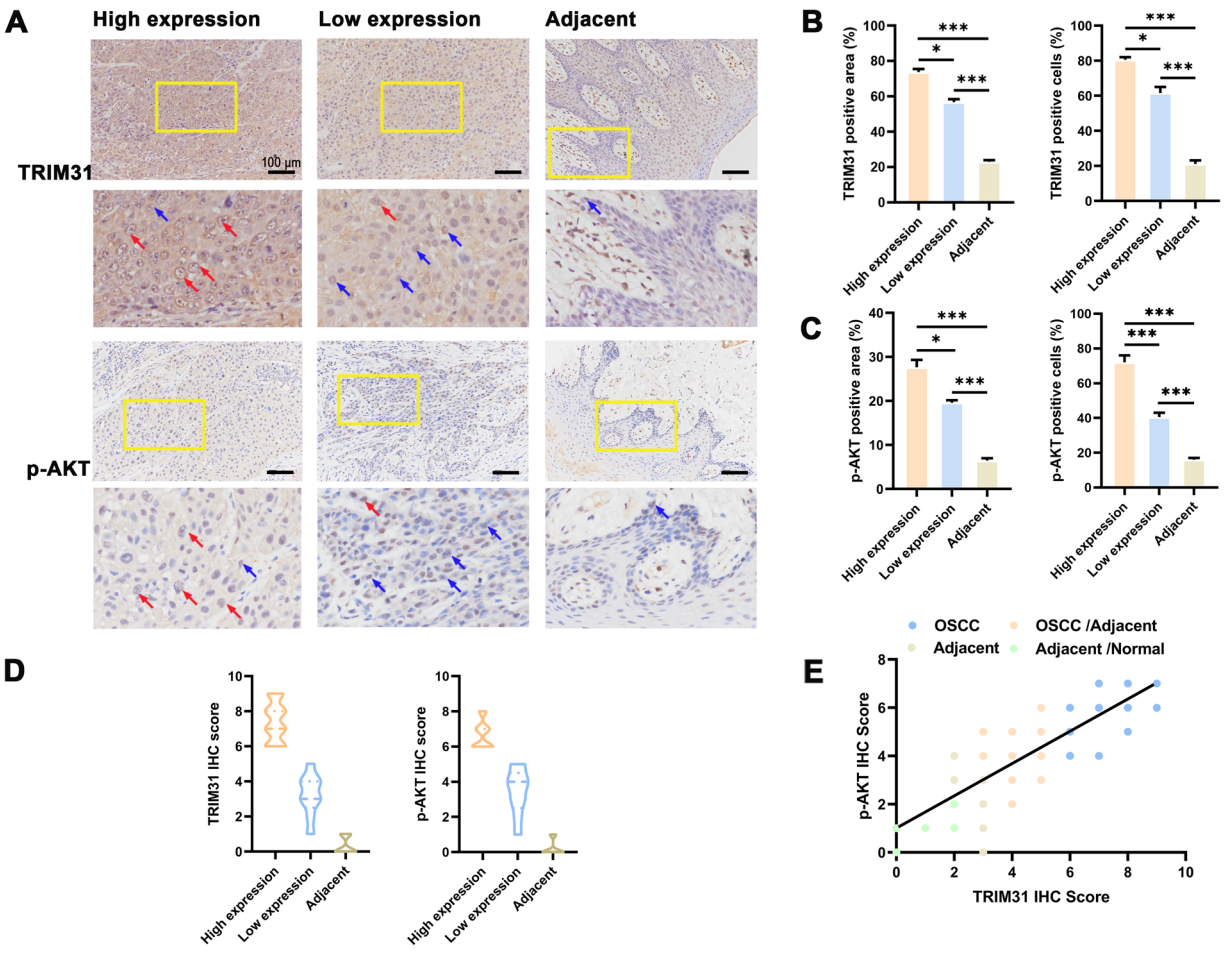

Figure 1. Evaluation of TRIM31 and p-AKT expression levels using OSCC tissue microarrays. A) Expression patterns of TRIM31 and p-AKT in OSCC (left two columns) and adjacent (right column) tissues detected by immunohistochemical staining (red arrows point to tumor cells with high expression of TRIM31/p-AKT, blue arrows point to lowly-expressing cells, ×200). B, C) Quantification of B) TRIM31 and C) p-AKT positively stained areas and cells in OSCC and adjacent tissues. D) Corresponding IHC staining scores and E) scatter plot analysis of the correlation between TRIM31 and p-AKT IHC scores. Notes: High expression-tumor tissue with high TRIM31/p-AKT expression; Low expression-tumor tissue with low TRIM31/p-AKT expression; Adjacent-adjacent tissue, Normal-normal tissue. *p<0.05, ***p<0.001

tently, the percentages of patients with increased TRIM31 expression were higher among those presenting with worse clinical manifestations (Supplementary Figures S1A–S1D). Furthermore, Spearman correlation analysis revealed a positive correlation between OSCC clinical presentations and TRIM31 expression (Table 2). Analysis of distant metastasis of OSCC was not performed due to missing data.

The successful construction of OSCC cell models with TRIM31 expression down- and up-regulation. TRIM31 protein expression in four human OSCC cell lines (Fadu, HSC6, CAL27, and HSC3) was analyzed by western blotting assay; the HOEC oral epithelial cell line was used as a control. In comparison to the control, maximum TRIM31 expression was detected in CAL27 cells, while HSC6 cells only showed slightly elevated TRIM31 expression (Supplementary Figure S2A). Next, TRIM31 levels were down- and up-regulated in CAL27 and HSC6 cells, respectively. Western blotting and qRT-PCR assays revealed clearly reduced TRIM31 protein and mRNA levels in CAL27 cells transfected with Sh-TRIM31s, with Sh-TRIM31-1 and Sh-TRIM31-2 achieving higher knockdown efficiencies (Supplementary Figures S2B, S2C). Additionally, HSC6 cells showed apparent enhancement of TRIM31 expression at both the protein and mRNA levels after TRIM31-CDS transfection (Supplementary Figures S2D, S2E).

TRIM31 regulates the malignant behaviors of OSCC cells via AKT signaling. To validate the important role of TRIM31 in the regulation of OSCC cell behaviors, *in vitro* CCK-8, Transwell, and scratch assays were first performed using CAL27 cells following different treatments. TRIM31 interference remarkably decreased CAL27 cell proliferation and invasion ability (Figures 2A, 2B). Quantitatively,

cell invasion was approximately 60% lower in Sh-TRIM31-transfected cells compared to that in Sh-NC-transfected cells (Figure 2B). TRIM31 knockdown evidently prohibited cell migration, with the migration rate of Sh-TRIM31-transfected cells decreased by around 50% relative to Sh-NC-transfected cells (Figure 2C). As illustrated in Figure 2D, although there was no apparent effect of TRIM31 inhibition on AKT protein expression, p-AKT levels were markedly lower in Sh-TRIM31-transfected cells than in Sh-NC-transfected cell.

In contrast, aggressive OSCC cell phenotypes and intracellular AKT phosphorylation were significantly enhanced in HSC6 cells after transfection of TRIM31-CDS (Figures 3A–3D). Relative to control cells transfected with empty vectors, cell invasion, migration, and AKT phosphorylation was increased by approximately 25%, 25%, and 100%, respectively, in TRIM31-CDS-transfected cells (Figures 3B–3D).

To further explore the function of p-AKT in TRIM31 regulation, TRIM31-CDS-transfected HSC6 cells were treated with the AKT inhibitor (LY294002).

As shown in Figures 3A–3D, the addition of LY294002 remarkably weakened the effect of TRIM31 overexpression on malignant cell behaviors, as well as intracellular AKT phosphorylation. Treatment of untransfected HSC6 cells with LY294002 alone yielded similar inhibitory effects on the analyzed phenotypes (Figures 3A–3D).

Table 2. Correlation between TRIM31 expression and OSCC clinical manifestations analyzed by Spearman correlation test.

Clinical manifestation	TRIM31 expression in the OSCC tissues		
	Spearman correlation	95% CI	p-value
Tumor size	0.387	0.632~0.072	0.015
T classification	0.378	0.625~0.061	0.018
TNM stage (AJCC)	0.470	0.689~0.171	0.003
Lymph node metastasis	0.433	0.664~0.127	0.006

Abbreviation: AJCC-American Joint Committee on Cancer

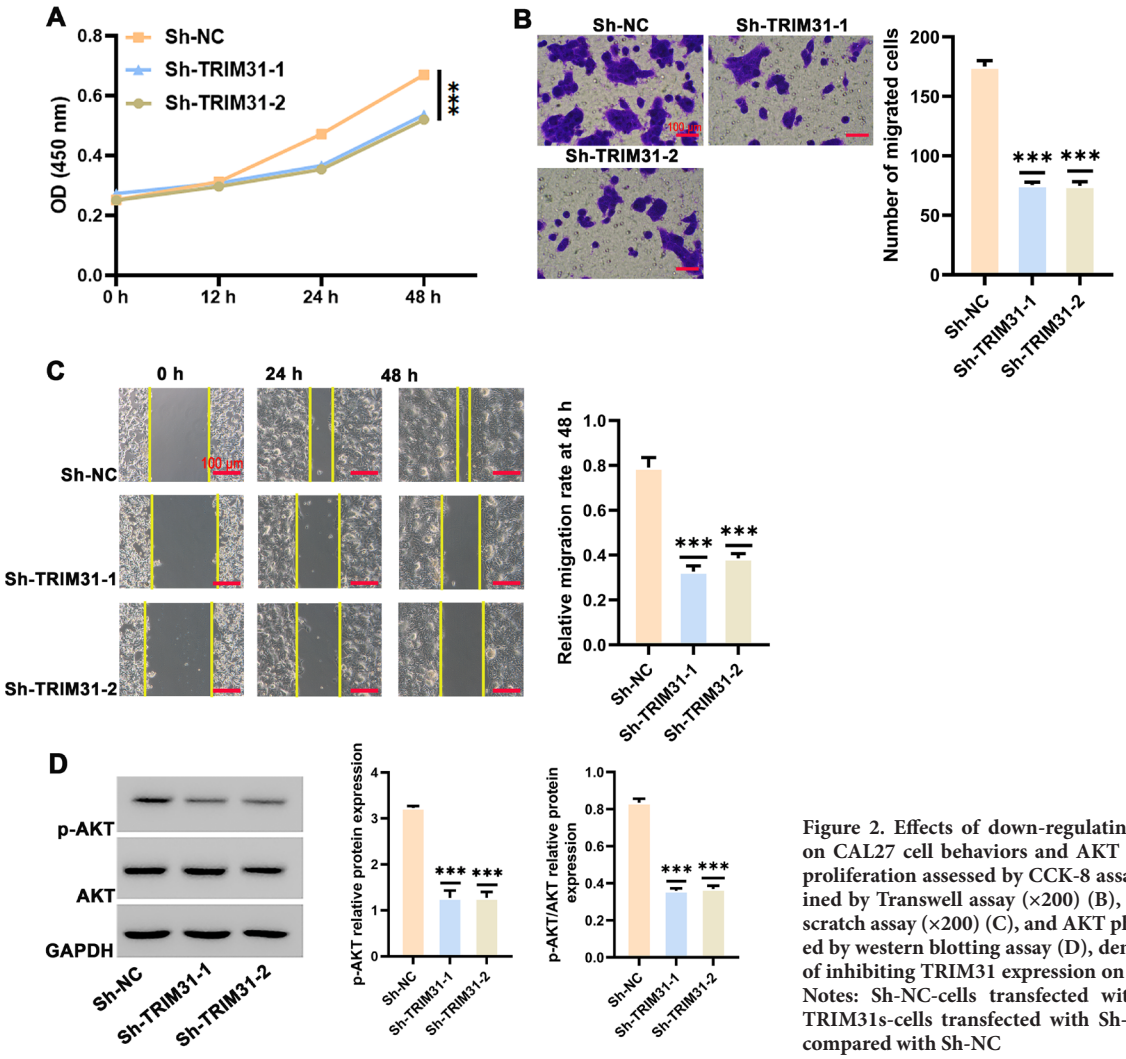

Figure 2. Effects of down-regulating TRIM31 expression on CAL27 cell behaviors and AKT phosphorylation. Cell proliferation assessed by CCK-8 assay (A), invasion examined by Transwell assay (×200) (B), migration assessed by scratch assay (×200) (C), and AKT phosphorylation detected by western blotting assay (D), demonstrating the effects of inhibiting TRIM31 expression on CAL27 cell behaviors. Notes: Sh-NC-cells transfected with empty vector; Sh-TRIM31s-cells transfected with Sh-TRIM31s. ***p<0.001 compared with Sh-NC

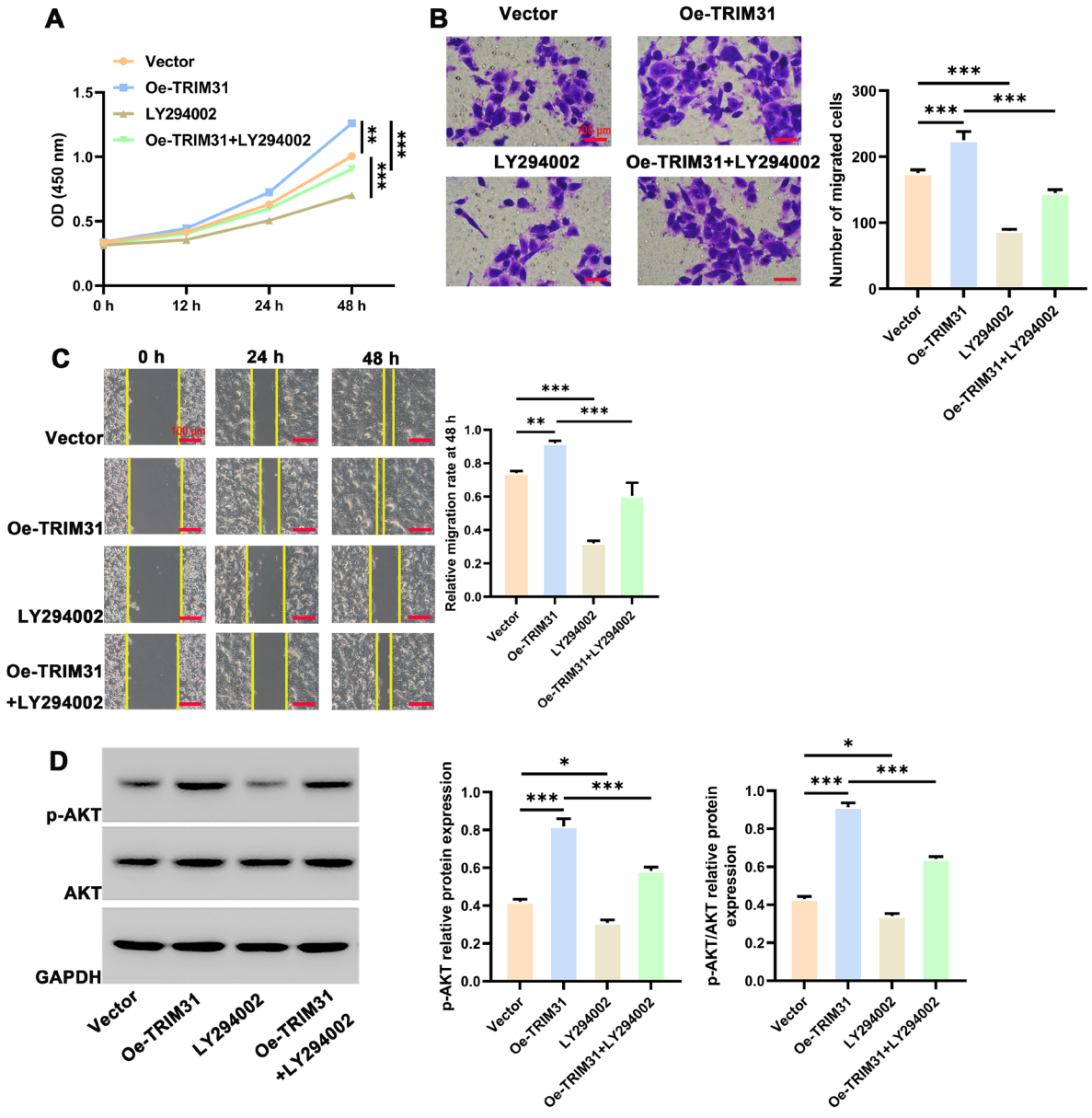

Figure 3. The effects of up-regulating of TRIM31 expression on HSC6 cell behaviors and intracellular p-AKT levels. Cell proliferation detected by CCK-8 assay (A), invasion assessed by Transwell assay (×200) (B), migration examined by scratch assay (×200) (C), and AKT phosphorylation determined by western blotting assay (D), showing the effects of overexpressing TRIM31 on HSC6 cells. Notes: Vector-cells transfected with empty vector; Oe-TRIM31-cells transfected with TRIM31-CDS; LY294002-cells treated with LY294002 (AKT inhibitor) alone; Oe-TRIM31+LY294002-cells transfected with TRIM31-CDS and treated with LY294002. *p<0.05, **p<0.01, ***p<0.001

The TRIM31/AKT pathway regulates OSCC growth *in vivo*. To verify the role of the TRIM31/AKT pathway in regulating OSCC development *in vivo*, we constructed nude mouse xenograft cancer models by injecting the animals with OSCC cells treated with empty vector (Vector), Sh-TRIM31, Sh-TRIM31 plus AKT activator (Sh-TRIM31+SC-79), TRIM31-CDS (Oe-TRIM31), and TRIM31-CDS plus AKT inhibitor (Oe-TRIM31+LY294002) (Figure 4A). The appearance of tumors harvested from each group is shown in Figure 4B. Tumor cells from all groups appeared as disorderly nest-like structures, as demonstrated by hematoxylin and eosin staining (Figure 4C).

Tumors from mice in the Vector group were heavier and had larger volumes than those from the Sh-TRIM31 group (Figures 4B, 4D, 4E). Specific IHC staining of tumor tissue samples showed that TRIM31 expression was lowest in the Sh-TRIM31 group (Figure 4F). Additionally, compared with the Sh-TRIM31 group, the Sh-TRIM31+SC-79 group

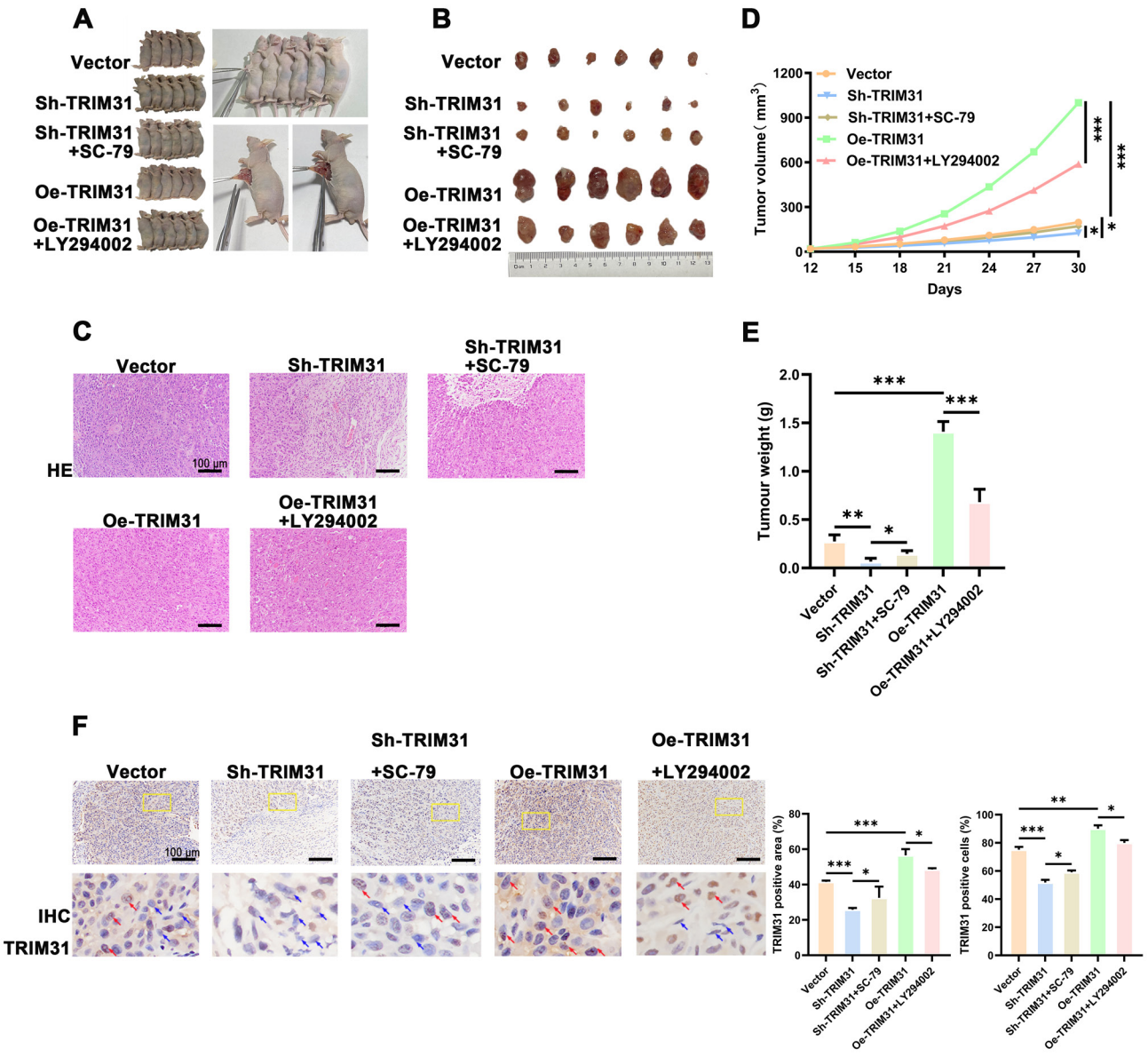

Figure 4. Role of the TRIM31/AKT pathway in regulating tumor growth in nude mouse xenograft tumor models. A) Grouping of xenograft tumor models following different treatments and harvesting of tumor tissues. The appearance (B) and hematoxylin-eosin (HE) staining (×200) (C) of tumor tissues from each group. Volumes (D), weights (E), and immunohistochemical (IHC) staining of TRIM31 (red arrows point to tumor cells with high expression of TRIM31, blue arrows point to lowly-expressing cells, ×200) and the percentages of the positively stained areas and cells of tumor tissue samples from each group (F). Notes: Vector-cells transfected with empty vector; Sh-TRIM31-cells transfected with Sh-TRIM31; Sh-TRIM31+SC-79-cells transfected with Sh-TRIM31 and treated with SC-79 (AKT activator); Oe-TRIM31-cells transfected with TRIM31-CDS; Oe-TRIM31+LY294002-cells transfected with TRIM31-CDS and treated with LY294002 (AKT inhibitor). *p<0.05, **p<0.01, ***p<0.001

had increased tumor development and TRIM31 expression (Figures 4B, 4D–4F). Moreover, the Oe-TRIM31 group exhibited the most rapid tumor growth, the largest tumor weight, and the strongest TRIM31 protein expression (Figure 4B, 4D–4F); however, the apparent tumor-promoting effect of TRIM31 overexpression *in vivo* was largely ameliorated by AKT inhibitor, as indicated by analysis of mice from the Oe-TRIM31+LY294002 group (Figure 4B, 4D–4F).

TRIM31 modulates OSCC cell glycolysis via the regulation of AKT signaling. To assess the impacts of TRIM31 on OSCC cell glycolytic metabolism, glucose consumption, ATP generation, and lactate excretion were first measured in CAL27 cells following different treatments. As illustrated in Figures 5A–5C, TRIM31 interference clearly disturbed cellular glycolytic activity. Quantitatively, the values of the glycolysis-related indicators mentioned above were approxi-

mately 50% lower in the Sh-TRIM31-transfected cells than those in the Sh-NC-transfected cells. TRIM31 overexpression in HSC6 cells significantly increased glycolytic processes; values of glucose consumption, lactate production, and ATP production in TRIM31-CDS-transfected cells were approximately 1.3, 3, and 2 times those in control cells transfected with empty vector (Figures 5D–5F).

To clarify the function of p-AKT in TRIM31 regulation of cellular glycolytic capacity, TRIM31-CDS-transfected HSC6 cells were further treated with an AKT inhibitor (LY294002). LY294002 addition clearly diminished the glycolysis-promoting influence of TRIM31 overexpression (Figures 5D–5F). Moreover, treatment of untransfected HSC6 cells with LY294002 alone achieved similar inhibitory effects on glycolytic activity (Figures 5D–5F).

TRIM31-induced glycolysis is an important mechanism regulating OSCC cell behaviors. To determine whether TRIM31-induced glycolysis can regulate OSCC cell behaviors, *in vitro* GLUT1 and HK2 protein expression, CCK-8, Transwell, and scratching assays were first carried out using CAL27 cells following different treatments. As shown in Figure 6A, Sh-TRIM31-transfected CAL27 cells exhibited prominently decreased GLUT1 and HK2 expression levels, relative to those of cells transfected with empty vector. The reduction of these two glycolysis-related proteins was accompanied by significantly decreased cell proliferation, invasion, and migration abilities (Figures 6B–6D).

Compared with control HSC-6 cells transfected with empty vector, TRIM31-CDS-transfected cells demonstrated remarkably enhanced GLUT1 and HK2 expression levels, as well as more aggressive behaviors (Figures 6G, 6H). TRIM31-CDS-transfected cells were next treated with glycolysis inhibitor (2-DG). As illustrated in Figures 6G and 6H, 2-DG treatment clearly inhibited the positive effects of up-regulating TRIM31 on GLUT1 and HK2 expression, as well as on malignant cell behaviors. Similarly, the application of 2-DG on untreated HSC6 cells also exerted suppressive effects on the analyzed phenotypes (Figures 6G, 6H).

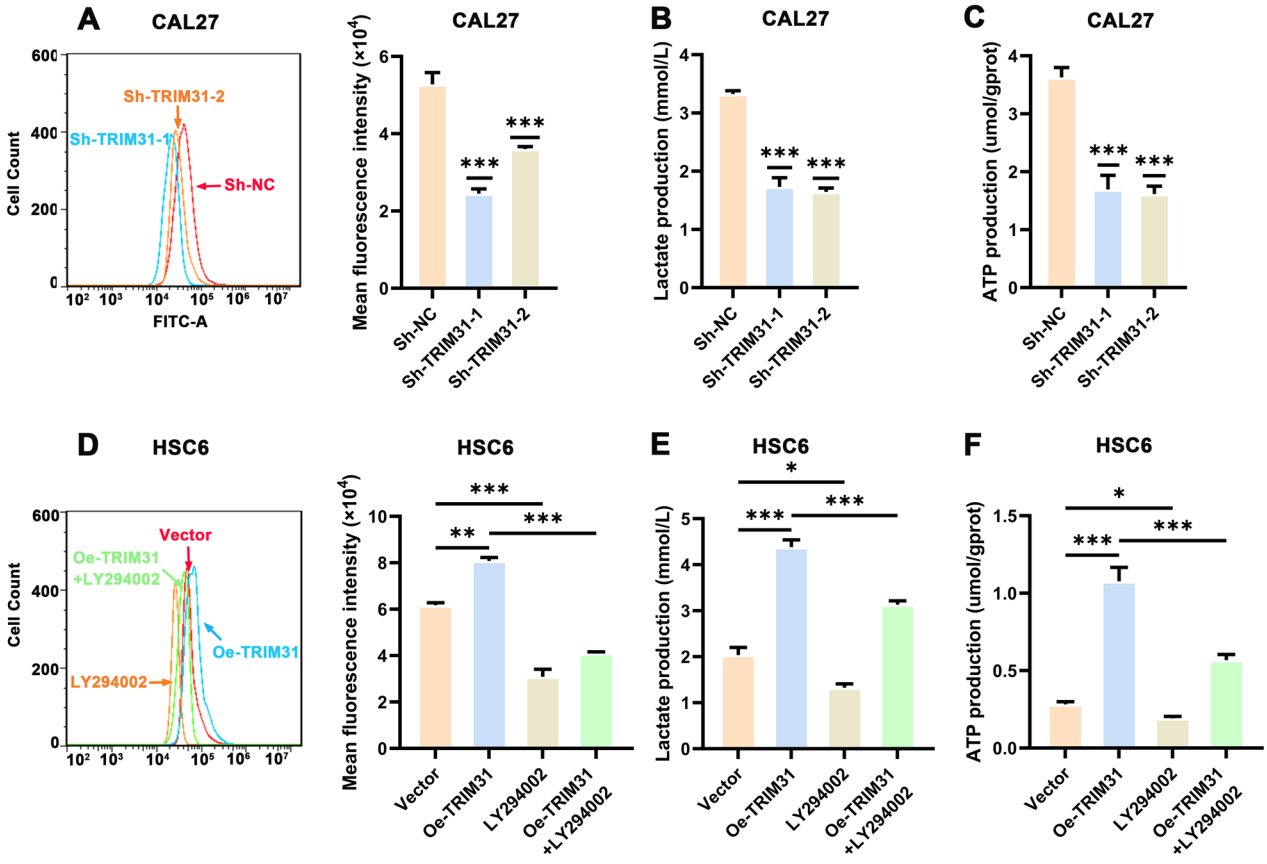

Figure 5. TRIM31/AKT pathway regulation of glycolytic metabolism in OSCC cells. A) Cellular glucose uptake measured by flow cytometry, B) lactate secretion evaluated by lactate detection kit, and (C) ATP production quantified by ATP determination kit, demonstrating the effects of down-regulating TRIM31 expression on CAL27 cell glycolysis. D–F) The above indicators were used to assess the effects of up-regulating the TRIM31/AKT pathway, with and without AKT inhibitor, on the glycolysis-related activities of HSC6 cells. Notes: Sh-NC-cells transfected with empty vector; Sh-TRIM31s-cells transfected with Sh-TRIM31s; Vector-cells transfected with empty vector; Oe-TRIM31-cells transfected with TRIM31-CDS; LY294002-cells treated with LY294002 (AKT inhibitor) alone; Oe-TRIM31+LY294002-cells transfected with TRIM31-CDS and treated with LY294002. *p<0.05, **p<0.01, ***p<0.001

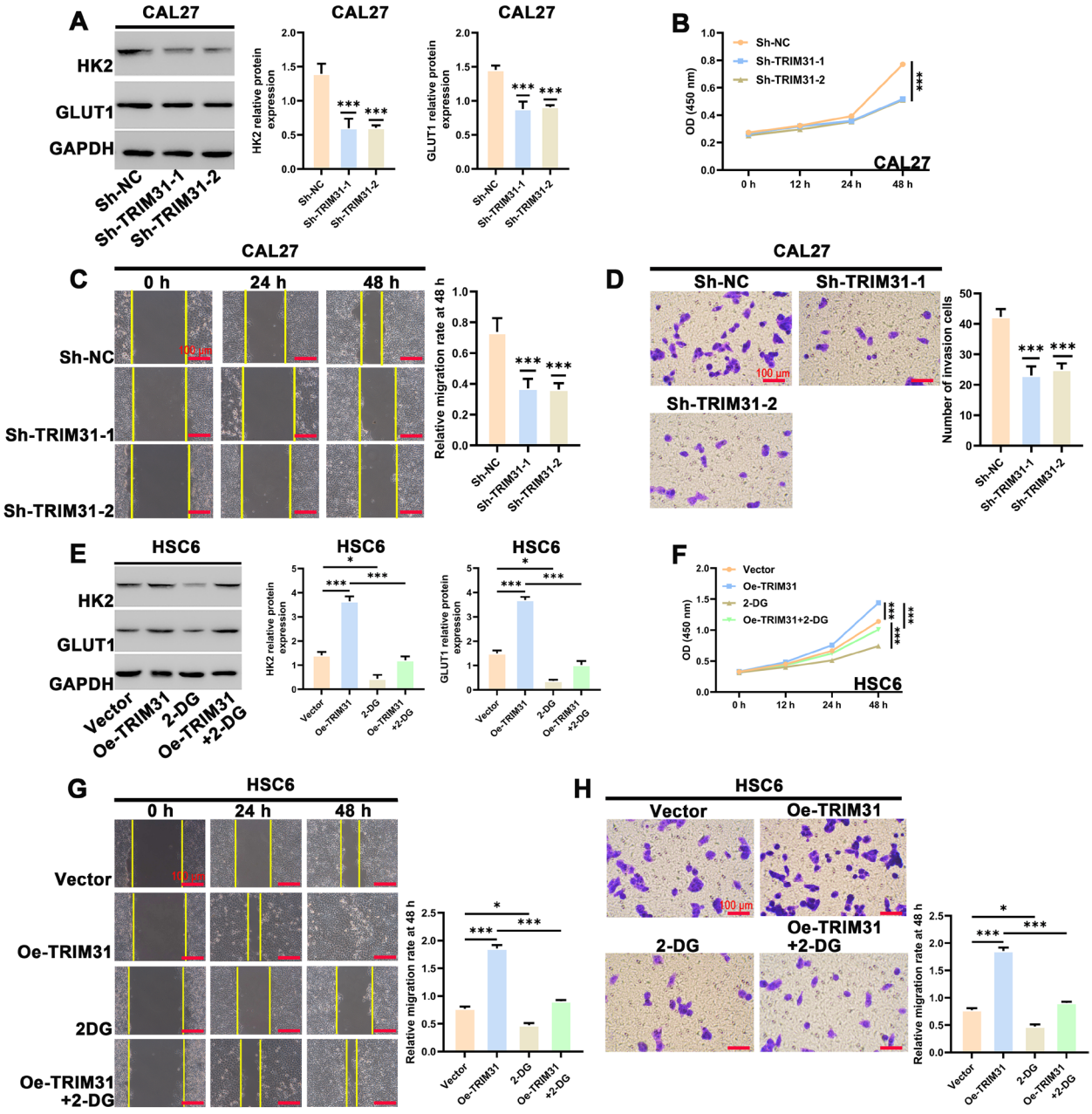

Figure 6. The effect of TRIM31 on OSCC cell behaviors via regulation of glycolysis. A) HK2 and GLUT1 protein levels detected by western blotting, B) cell proliferation measured by CCK-8 assay, C) cell migration examined by scratch assay (×200), and D) cell invasion assessed by Transwell assay (×200), showing the effects of reducing TRIM31 expression on the glycolysis and subsequent behaviors of CAL27 cells. E–H) The above indicators were used to evaluate the effects of enhancing TRIM31 expression on the glycolytic activities and behaviors of HSC6 cells in the presence and absence of a glycolysis inhibitor. Notes: Sh-NC-cells transfected with empty vector; Sh-TRIM31s-cells transfected with Sh-TRIM31s; Vector-cells transfected with empty vector; Oe-TRIM31-cells transfected with TRIM31-CDS; 2-DG-cells treated with 2-DG (glycolysis inhibitor) alone; Oe-TRIM31+2-DG-cells transfected with TRIM31-CDS and treated with 2-DG. *p<0.05, **p<0.01, ***p<0.001

Discussion

OSCC is categorized as carcinoma resulting from the epithelium covering the oral cavity, such as the tongue, gingiva, and floor of the mouth [19]. Currently, OSCC is the sixth most common epithelial neoplasm occurring in the neck and head area [19, 20]. Despite great improvements in therapeutic approaches over the decades, the long-term survival rate of patients with OSCC remains suboptimal, and the pathogenesis of the disease remains unclear [21].

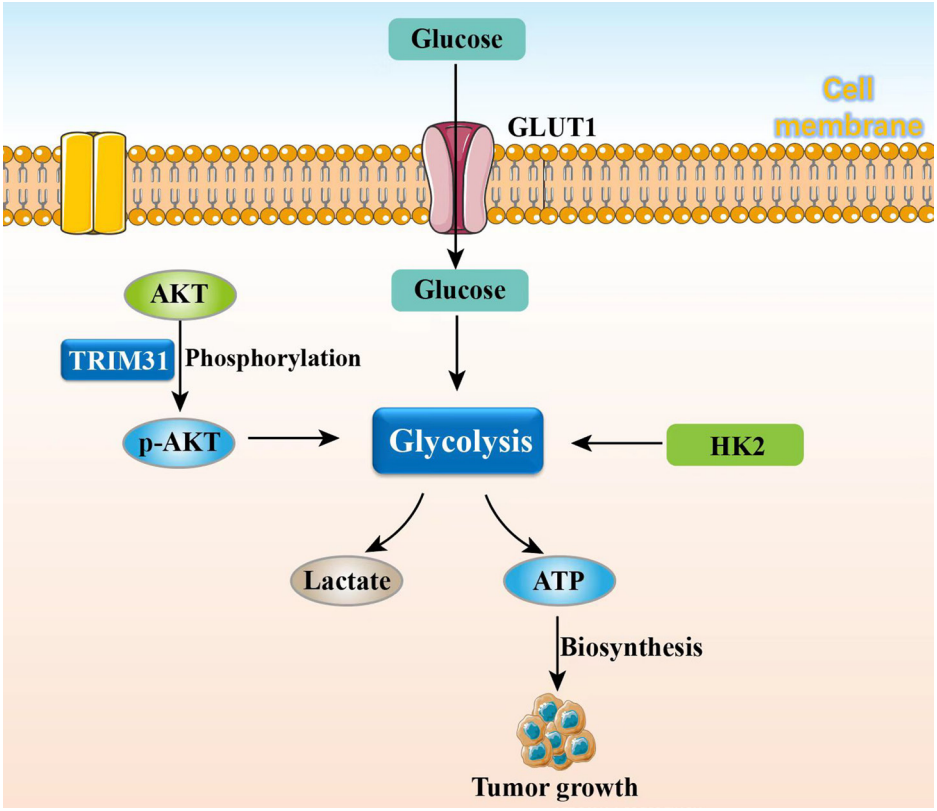

Figure 7. The possible mechanism by which TRIM31 promotes OSCC progression through upregulating AKT phosphorylation and subsequent glycolysis.

To improve the effectiveness of treatment, it is necessary to identify precise diagnostic biomarkers and therapeutic targets [22].

TRIM31 acts as a crucial regulating factor in cancer development, and its involvement in breast cancer [7], glioblastoma [5], pancreatic cancer [23], and gastrointestinal cancer [24] has been proven; however, knowledge of the role of TRIM31 in OSCC is incomplete. In the present study, IHC staining of human OSCC tissue microarrays revealed significantly stronger TRIM31 expression in tumor samples than that in adjacent tissue. Moreover, patients presenting with higher TRIM31 levels exhibited worse clinical manifestations. Given the close relationship between TRIM31 and the clinical invasiveness of OSCC, TRIM31 has the potential as a diagnostic marker for the disease. Additionally, *in vitro* and *in vivo* examinations showed that TRIM31 up-regulation enhanced the invasion, growth, and migration activities of OSCC cells, while TRIM31 down-regulation mitigated these aggressive phenotypes. The above results indicate that TRIM31 may contribute to OSCC development.

Previous studies have demonstrated the participation of TRIM31/AKT signaling in regulating tumor cell malignant behaviors; for example, p-AKT is a key downstream regulator of TRIM31 in the progression of breast cancer, glioblastoma, and gallbladder cancer [5, 9, 15]. Similarly, our findings suggest that TRIM31 and p-AKT expression levels in OSCC tumor tissues are consistent, and alteration of AKT phosphorylation was positively correlated with up- and down-regulation of TRIM31 expression in OSCC cells. In addition, treatment with the AKT inhibitor (LY294002) decreased TRIM31-induced cell aggressiveness, while the AKT activator (SC-79) reversed the negative effect of TRIM31 knockdown on tumor growth. Therefore, p-AKT may be a crucial signaling pathway in the regulatory mechanism of TRIM31 in influencing OSCC development. As TRIM31 improved the *in vitro* invasiveness of OSCC cells and *in vivo* tumor growth through activating AKT phosphorylation, the TRIM31/AKT pathway represents a possible treatment target for individuals with OSCC.

Glycolysis is a major cellular metabolic process involving the conversion of glucose to lactate and subsequent ATP production, which provides the necessary energy for cell functions [25]. Glycolysis is the primary source of ATP energy for tumor cells in aerobic situations [26–28]. Relative to normal cells, cancer cells often exhibit an increased demand for energy, and present with an enhanced glycolytic capacity, featuring accelerated glucose uptake and higher production of lactate and ATP, owing to their rapid growth

and proliferation [29–31]. As glucose metabolism reprogramming is crucial for cancer cell survival after surgical resection and drug administration [32], therapies targeting glycolysis represent a valuable clinical approach [33]. Many studies have validated AKT signaling as an essential upstream regulator of glycolytic metabolism in various tumor cells [10, 11]. For example, antisense RNA1 of HIF1α (HIF1A-AS1) and polo-like kinase 1 (PLK1) stimulate glycolysis via AKT signaling, thus regulating tumorigenesis of pancreatic cancer and laryngeal squamous cell carcinoma, respectively [34, 35]. In this study, the reduced AKT phosphorylation after the knockdown of TRIM31 was followed by a decrease in glucose uptake, as well as lower ATP and lactate production, in OSCC cells. In contrast, the increased p-AKT levels following TRIM31 overexpression enhanced glycolysis-related phenotypes, while treatment with an AKT inhibitor (LY294002) rescued the impacts of TRIM31 up-regulation. Therefore, we speculate that glycolysis may be a downstream mechanism in TRIM31/AKT pathway regulation of OSCC behaviors.

GLUT1 and HK2 are two key functional proteins in glycolysis. Specifically, GLUT1 is a transmembrane protein, which transports glucose into cells through facilitative diffusion [36], while HK2 acts as a vital glycolytic enzyme catalyzing the transformation of glucose into glucose-6-phosphate [37]. Previous investigations of endometrial cancer, pancreatic cancer, hepatocellular carcinoma, and glioblastoma have demonstrated that GLUT1 and HK2 levels can be induced by various factors and that this process is a crucial step in enhancing glucose metabolism and subsequent cancer invasiveness [36, 38–40]. Our findings also showed a positive relationship between TRIM31, GLUT1, and HK2 expression levels and OSCC cell malignant activities, and the cancer-promoting function of TRIM31 was subdued by treatment with the glycolytic inhibitor, 2-DG. These results implicate glycolysis as a potentially pivotal biological process in transmitting "regulatory information" from TRIM31 to OSCC cell behaviors.

In summary, our data indicate that: first, p-AKT is a crucial downstream signaling factor in TRIM31 regulation of OSCC development; second, the TRIM31/AKT pathway regulates OSCC cell glycolysis; and third, glycolysis is an important process through which TRIM31 regulates OSCC cell behaviors. Hence, TRIM31 may induce OSCC progression by enhancing AKT signaling and subsequent cellular glycolysis.

The present study has some limitations. As only human OSCC tissue microarrays, with a limited number of cases and clinical information were used, more OSCC specimens, with complete data on patient clinical characteristics, manifestations, treatments, and prognosis, are necessary for future studies to validate our findings. Besides, although our findings suggest the TRIM31/AKT pathway and glycolysis as potential diagnostic and therapeutic targets of OSCC, further in-depth research, focusing on the underlying mechanism, such as related protein functional sites and detailed biological steps, is still required.

In conclusion, TRIM31 may promote OSCC development by activating the AKT phosphorylation and subsequent glycolytic metabolism. These findings provide potentially important insights into OSCC pathological and molecular processes.

Supplementary information is available in the online version of the paper.

Acknowledgments: This work is supported by the research project of the Shanghai Municipal Committee of Science and Technology (No.21ZR1455600).

References

[1] HAN Y, XIA K, SU T. Exploration of the Important Role of Microfibril-Associated Protein 4 Gene in Oral Squamous Cell Carcinoma. Med Sci Monit 2021; 27: e931238. https://doi.org/10.12659/MSM.931238

[2] WU C, YANG M, CHEN H. Inhibition effect of miR-150 on the progression of oral squamous cell carcinoma by data analysis model based on independent sample T-test. Saudi J Biol Sci 2020; 27: 599–605. https://doi.org/10.1016/j.sjbs.2019.11.022

[3] ZHOU J, LI H, CHENG B, CAO R, ZOU F et al. Derivation and Validation of a Prognostic Scoring Model Based on Clinical and Pathological Features for Risk Stratification in Oral Squamous Cell Carcinoma Patients: A Retrospective Multicenter Study. Front Oncol 2021; 11: 652553. https://doi.org/10.3389/fonc.2021.652553

[4] WANG H, YAO L, GONG Y, ZHANG B. TRIM31 regulates chronic inflammation via NF-κB signal pathway to promote invasion and metastasis in colorectal cancer. Am J Transl Res 2018; 10: 1247–1259. https://doi.org/10.3892/etm.2020.8782

[5] FAN MD, ZHAO XY, QI JN, JIANG Y, LIU BY et al. TRIM31 enhances chemoresistance in glioblastoma through activation of the PI3K/Akt signaling pathway. Exp Ther Med. 2020; 20: 802–809. https://doi.org/10.3892/etm.2020.8782

[6] SHI G, LV C, YANG Z, QIN T, SUN L et al. TRIM31 promotes proliferation, invasion and migration of glioma cells through Akt signaling pathway. Neoplasma 2019; 66: 727–735. https://doi.org/10.4149/neo_2019_190106N21

[7] GUO Y, LI Q, ZHAO G, ZHANG J, YUAN H et al. Loss of TRIM31 promotes breast cancer progression through regulating K48- and K63-linked ubiquitination of p53. Cell Death Dis 2021; 12: 945. https://doi.org/10.1038/s41419-021-04208-3

[8] GUO P, MA X, ZHAO W, HUAI W, LI T et al. TRIM31 is upregulated in hepatocellular carcinoma and promotes disease progression by inducing ubiquitination of TSC1-TSC2 complex. Oncogene 2018; 37: 478–488. https://doi.org/10.1038/onc.2017.349

[9] LI H, ZHANG Y, HAI J, WANG J, ZHAO B et al. Knockdown of TRIM31 suppresses proliferation and invasion of gallbladder cancer cells by down-regulating MMP2/9 through the PI3K/Akt signaling pathway. Biomed Pharmacother 2018; 103: 1272–1278. https://doi.org/10.1016/j.biopha.2018.04.120

[10] XU ZX, TAN JW, XU H, HILL CJ, OSTROVSKAYA O et al. Caspase-2 promotes AMPA receptor internalization and cognitive flexibility via mTORC2-AKT-GSK3β signaling. Nat Commun 2019; 10: 3622. https://doi.org/10.1038/s41467-019-11575-1

[11] NAM S, GUPTA VK, LEE HP, LEE JY, WISDOM KM et al. Cell cycle progression in confining microenvironments is regulated by a growth-responsive TRPV4-PI3K/Akt-p27Kip1 signaling axis. Sci Adv 2019; 5: eaaw6171. https://doi.org/10.1126/sciadv.aaw6171

[12] XU L, CHEN J, JIA L, CHEN X, AWALEH MOUMIN F et al. SLC1A3 promotes gastric cancer progression via the PI3K/AKT signalling pathway. J Cell Mol Med 2020; 24: 14392–14404. https://doi.org/10.1111/jcmm.16060

[13] LIANG L, CHEN Y, YU Y, PAN W, CUI Y et al. SLC25A18 has prognostic value in colorectal cancer and represses Warburg effect and cell proliferation via Wnt signaling. Am J Cancer Res 2020; 10: 1548–1567.

[14] LI Y, WANG J, WANG F, WANG H, WANG J et al. Tissue microarray analysis reveals the expression and prognostic significance of phosphorylated AktThr308 in oral squamous cell carcinoma. Oral Surg Oral Med Oral Pathol Oral Radiol 2013; 116: 591–597. https://doi.org/10.1016/j.oooo.2013.06.031

[15] YANG Z, XU B, WU S, YANG W, LUO R et al. Exosomal microRNA-551b-3p from bone marrow-derived mesenchymal stromal cells inhibits breast cancer progression via regulating TRIM31/Akt signaling. Hum Cell 2022; 35: 1797–1812. https://doi.org/10.1007/s13577-022-00753-x

[16] BARNES JM, KAUSHIK S, BAINER RO, SA JK, WOODS EC et al. A tension-mediated glycocalyx-integrin feedback loop promotes mesenchymal-like glioblastoma. Nat Cell Biol 2018; 20: 1203–1214. https://doi.org/10.1038/s41556-018-0183-3

[17] FAN H, YUAN J, LI Y, JIA Y, LI J et al. MKL1-induced lncRNA SNHG18 drives the growth and metastasis of non-small cell lung cancer via the miR-211-5p/BRD4 axis. Cell Death Dis 2021; 12: 128. https://doi.org/10.1038/s41419-021-03399-z

[18] YU B, ZHANG Y, WU K, WANG L, JIANG Y et al. CD147 promotes progression of head and neck squamous cell carcinoma via NF-kappa B signaling. J Cell Mol Med 2019; 23: 954–966. https://doi.org/10.1111/jcmm.13996

[19] SU W, SUN S, WANG F, SHEN Y, YANG H. Circular RNA hsa_circ_0055538 regulates the malignant biological behavior of oral squamous cell carcinoma through the p53/Bcl-2/caspase signaling pathway. J Transl Med 2019; 17: 76. https://doi.org/10.1186/s12967-019-1830-6

[20] MANSOUR MA. Ubiquitination: Friend and foe in cancer. Int J Biochem Cell Biol 2018; 101: 80–93. https://doi.org/10.1016/j.biocel.2018.06.001

[21] FAN Q, WANG Q, CAI R, YUAN H, XU M. The ubiquitin system: orchestrating cellular signals in non-small-cell lung cancer. Cell Mol Biol Lett 2020; 25: 1. https://doi.org/10.1186/s11658-019-0193-6

[22] LEE C, CHOI YJ, JEON KJ, KIM DW, NAM W et al. Prognostic Implications of Combined Imaging and Histologic Criteria in Squamous Cell Carcinoma with Mandibular Invasion. J Clin Med 2020; 9: 1335. https://doi.org/10.3390/jcm9051335

[23] Yu C, Chen S, Guo Y, Sun C. Oncogenic TRIM31 confers gemcitabine resistance in pancreatic cancer via activating the NF-κB signaling pathway. Theranostics 2018; 8: 3224–3236. https://doi.org/10.7150/thno.23259

[24] TEMENA MA, ACAR A. Increased TRIM31 gene expression is positively correlated with SARS-CoV-2 associated genes TMPRSS2 and TMPRSS4 in gastrointestinal cancers. Sci Rep 2022; 12: 11763. https://doi.org/10.1038/s41598-022-15911-2

[25] HUANG J, GAO W, LIU H, YIN G, DUAN H et al. Up-regulated ANP32E promotes the thyroid carcinoma cell proliferation and migration via activating AKT/mTOR/HK2-mediated glycolysis. Gene 2020; 750: 144681. https://doi.org/10.1016/j.gene.2020.144681

[26] SCHWARTZ L, SUPURAN CT, ALFAROUK KO. The Warburg Effect and the Hallmarks of Cancer. Anticancer Agents Med Chem 2017; 17: 164–170. https://doi.org/10.2174/1871520616666161031143301

[27] ICARD P, SHULMAN S, FARHAT D, STEYAERT JM, ALIFANO M et al. How the Warburg effect supports aggressiveness and drug resistance of cancer cells? Drug Resist Updat 2018; 38: 1–11. https://doi.org/10.1016/j.drup.2018.03.001

[28] PASCALE RM, CALVISI DF, SIMILE MM, FEO CF, FEO F. The Warburg Effect 97 Years after Its Discovery. Cancers (Basel) 2020; 12: 2819. https://doi.org/10.3390/cancers12102819

[29] LIU YJ, FAN XY, WANG AD, XIA YZ, FU WR et al. LDHA Suppression Altering Metabolism Inhibits Tumor Progress by an Organic Arsenical. Int J Mol Sci 2019; 20: 6239. https://doi.org/10.3390/ijms20246239

[30] WU Z, GU D, WANG R, ZUO X, ZHU H et al. CircRIC8B regulates the lipid metabolism of chronic lymphocytic leukemia through miR199b-5p/LPL axis. Exp Hematol Oncol 2022; 11: 51. https://doi.org/10.1186/s40164-022-00302-0

[31] KUANG Q, LIANG Y, ZHUO Y, CAI Z, JIANG F et al. The ALDOA Metabolism Pathway as a Potential Target for Regulation of Prostate Cancer Proliferation. Onco Targets Ther 2021; 14: 3353–3366. https://doi.org/10.2147/OTT.S290284

[32] FUMAROLA C, PETRONINI PG, ALFIERI R. Impairing energy metabolism in solid tumors through agents targeting oncogenic signaling pathways. Biochem Pharmacol 2018; 151: 114–125. https://doi.org/10.1016/j.bcp.2018.03.006

[33] MARTINEZ-OUTSCHOORN UE, PEIRIS-PAGÉS M, PESTELL RG, SOTGIA F, LISANTI MP. Cancer metabolism: a therapeutic perspective. Nat Rev Clin Oncol 2017; 14: 113. https://doi.org/10.1038/nrclinonc.2017.1

[34] XU F, HUANG M, CHEN Q, NIU Y, HU Y et al. LncRNA HIF1A-AS1 Promotes Gemcitabine Resistance of Pancreatic Cancer by Enhancing Glycolysis through Modulating the AKT/YB1/HIF1α Pathway. Cancer Res 2021; 81: 5678–5691. https://doi.org/10.1158/0008-5472

[35] GAO W, ZHANG Y, LUO H, NIU M, ZHENG X et al. Targeting SKA3 suppresses the proliferation and chemoresistance of laryngeal squamous cell carcinoma via impairing PLK1-AKT axis-mediated glycolysis. Cell Death Dis 2020; 11: 919. https://doi.org/10.1038/s41419-020-03104-6

[36] ZHANG Z, LI X, YANG F, CHEN C, LIU P et al. DHHC9-mediated GLUT1 S-palmitoylation promotes glioblastoma glycolysis and tumorigenesis. Nat Commun 2021; 12: 5872. https://doi.org/10.1038/s41467-021-26180-4

[37] JIAO L, ZHANG HL, LI DD, YANG KL, TANG J et al. Regulation of glycolytic metabolism by autophagy in liver cancer involves selective autophagic degradation of HK2 (hexokinase 2). Autophagy 2018; 14: 671–684. https://doi.org/10.1080/15548627.2017.1381804

[38] DONG P, XIONG Y, KONNO Y, IHIRA K, KOBAYASHI N et al. Long non-coding RNA DLEU2 drives EMT and glycolysis in endometrial cancer through HK2 by competitively binding with miR-455 and by modulating the EZH2/miR-181a pathway. J Exp Clin Cancer Res 2021; 40: 216. https://doi.org/10.1186/s13046-021-02018-1

[39] YU T, LI G, WANG C, GONG G, WANG L et al. MIR210HG regulates glycolysis, cell proliferation, and metastasis of pancreatic cancer cells through miR-125b-5p/HK2/PKM2 axis. RNA Biol 2021; 18: 2513–2530. https://doi.org/10.1080/15476286.2021.1930755

[40] Yu Q, Dai W, Ji J, Wu L, Feng J et al. Sodium butyrate inhibits aerobic glycolysis of hepatocellular carcinoma cells via the c-myc/hexokinase 2 pathway. J Cell Mol Med 2022; 26: 3031–3045. https://doi.org/10.1111/jcmm.17322